Optics Letters

High-order orbital angular momentum mode conversion based on a chiral long period fiber grating inscribed in a ring core fiber

ZHENG HUANG,[1,2] ZHIYONG BAI,[1,2,*] RUI LIU,[1,2] LUPING WU,[1,2] JIANJUN RAN,[1,2] ZIKAI CHEN,[1,2] GUOXUAN ZHU,[1,2] SHEN LIU,[1,2] CHANGRUI LIAO,[1,2] AND YIPING WANG[1,2]

[1] *Key Laboratory of Optoelectronic Devices and Systems of Ministry of Education and Guangdong Province, College of Physics and Optoelectronic Engineering, Shenzhen University, Shenzhen 518060, China*
[2] *Shenzhen Key Laboratory of Photonic Devices and Sensing Systems for Internet of Things, Guangdong and Hong Kong Joint Research Centre for Optical Fibre Sensors, Shenzhen University, Shenzhen 518060, China*
**Corresponding author: baizhiyong@szu.edu.cn*

Received 5 July 2022; revised 30 August 2022; accepted 26 September 2022; posted 27 September 2022; published 11 October 2022

A chiral long period fiber grating (CLPFG) was designed according to the phase-matching condition and conservation law of angular momentum, and was inscribed in a ring core fiber (RCF). This CLPFG was used to directly excite the ±2nd- and ±3rd-order orbital angular momentum (OAM) modes. The coupling efficiency of the OAM mode is up to 98.7% and the insertion loss is within 0.5 dB. The uniformity of the annular mode intensity distribution, polarization characteristics, and the mode purity of coupled OAM modes were investigated in detail. Results show that the coupled high-order OAM modes possess a relative uniform annular intensity distribution, its mode purity is up to 93.2%, and the helical phase modulation is independent on the polarization state of incident light. These results indicate that the RCF-based CLPFG is an ideal OAM mode converter for future high-capacity optical fiber communication systems.

https://doi.org/10.1364/OL.469373

With the vigorous development of information business, the transmission capacity of the single-mode optical fiber communication system (OFCS) has approached the nonlinear Shannon limit. Various degrees of freedom of the light wave, such as amplitude, frequency, polarization, and phase, have been developed and used to their limit through various technologies [1]. As a new degree of freedom, orbital angular momentum (OAM) has infinite dimensional orthogonality in theory. The mode division multiplexing technology based on the OAM mode [2] is one of the candidate technologies for the new generation of high-capacity optical fiber communication systems (HCOFCS). However, OAM modes cannot transmit over long distance in the commercial cylindrical few-mode fiber (FMF) because they can degenerate into linear polarization modes [3]. This results in the non-uniform annular intensity distribution and low purity of the OAM mode, which increases inter mode cross talk and the difficulty of mode demodulation in OFCS [4]. Thus, the ring core fiber (RCF) is designed and fabricated to solve the difficulty of long-distance transmission of the OAM mode [5], which is an important transmission medium for future HCOFCS.

To develop HCOFCS, the generation and regulation of OAM modes are the urgent problems. In the current HCOFCS based on a refractory ceramic fiber (RCF), OAM modes are mainly generated by using a free-spatial system such as spatial light modulators [6], which possess good flexibility. However, the high insertion loss and coupling difficulty are two common drawbacks for the method. Compared with free-spatial generators, the fiber-based OAM mode generators [7–10] are suitable for HCOFCS due to the advantages of low insertion loss, small volume, light weight, flexible use, and complete compatibility. At present, fiber-based OAM mode generators are mainly realized in FMF. Nevertheless, except for the ±1st-order OAM mode, the annular intensity distribution of the obtained higher-order OAM modes is non-uniform. Meanwhile, the mode mismatch exists in the coupling process between the FMF and the RCF due to the structural differences. In the work of RCF-based OAM mode generators, N. Bozinovic *et al.* [11] reported the excitation of 1st-order OAM mode by using a mechanically induced long period fiber grating (LPFG). However, the resonant wavelength and resonant depth of this LPFG were unstable under the influence of pressure, and the ±1st-order OAM mode could only be realized. Yang *et al.* [12] realized the excitation of higher-order OAM modes in tilted fiber Bragg grating. However, the obtained higher-order OAM modes had non-uniform annular intensity distribution and they were reflected from tilted fiber Bragg grating and so could not be directly connected to HCOFCS due to the lack of an all-fiber coupler for supporting OAM modes. In addition, in the above two technologies, OAM modes cannot be directly generated, but require the assistance of phase modulation equipment such as a polarization controller.

In this Letter, an OAM mode generator based on chiral long period fiber grating (CLPFG) inscribed in an RCF is realized for the first time, to the best of our knowledge. This CLPFG can directly excite OAM modes due to the modulation characteristic. According to the phase-matching condition and conservation law of angular momentum, we systematically designed this

CLPFG to achieve excitation of ±2nd- and ±3rd-order OAM modes. The coupled OAM modes have uniform intensity distribution and high purity because the RCF can support the OAM mode transmission.

In CLPFG, there is either the eccentric core of the originally used fiber or the imperfect cylindrical symmetry of the structure [13]. Simultaneously, to realize the excitation of higher-order modes in CLPFG, the high-order harmonic term needs to be considered [14,15]. Therefore, the refractive index modulation can be expressed as

$$\Delta N(r,\varphi,z) = \Delta N_0(r)\sum_{q=-\infty}^{\infty} s_q \exp\{i\cdot q\cdot m\cdot C(\varphi - C\cdot 2\pi z/\Lambda)\}, \tag{1}$$

where z represents the axial position along the CLPFG on the optical fiber, and ΔN_0 represents the maximum refractive index modulation. Here, m represents the rotational symmetry of the grating modulation cross section ($m = 1$ in this work due to the modulation of CLPFG); $C = +1$ and $C = -1$ represent the left-chirality CLPFG (L-CLPFG) and right-chirality CLPFG (R-CLPFG), respectively; q and s_q are the order and Fourier coefficients, respectively; Λ and φ represents the pitch of CLPFG and azimuth, respectively. According to Eq. (1), the phase-matching condition and conservation law of angular momentum [16] should modified as

$$n_h - n_f = q\cdot \lambda/\Lambda, \tag{2}$$

$$j_h - j_f = q\cdot C, \tag{3}$$

where n_f and n_h, j_f and j_h represent the effective refractive index and angular momentum of the fundamental mode and the exited high-order mode, respectively. Here, λ represents the resonant wavelength of CLPFG.

According to the Eqs. (2) and (3), for obtaining high-order OAM modes, the high-order diffraction grating instead of first-order diffraction of CLPFG is necessary. Corresponding to the second-harmonic term ($q = 2$), the grating pitch for excitation of the ±2nd-order OAM mode in CLPFG at a certain wavelength is twice that of the excitation of LP_{21} mode in LPFG. Similarly, the grating pitch for excitation of the ±3rd-order OAM mode is three times that of the LP_{31} mode, corresponding to the third-harmonic term ($q = 3$).

The optical fiber used in this work was an RCF with a step-index profile. The fiber end face was observed by scanning electron microscopy (SEM) and recorded in Fig. 1(a). The RCF consists of an annular guide layer and cladding. The refractive index difference between them is approximately 0.012, as shown in Fig. 1(b). The radius of cladding, and the inner and outer annular layers are 62.5 µm, 3.7 µm, and 7.6 µm, respectively. The RCF can support the transmission of OAM_0, $OAM_{\pm1}$, $OAM_{\pm2}$, and $OAM_{\pm3}$. By using the above parameters and finite element algorithm, the effective refractive index of all modes in the wavelength range of 1250–1650 nm were calculated and recorded, as shown in Fig. 1(c). Noted that the effective refractive index of the OAM mode can be approximately expressed by that of the linear polarization mode due to the superposition principle of the OAM mode. Then, combining with Eqs. (2) and (3), the dispersion curves of the mode coupling resonance wavelength between LP_{01} mode and LP_{21} mode, LP_{31} mode, ±2nd-order OAM mode, and ±3rd-order OAM mode with grating pitch were calculated respectively, as shown in Fig. 1(d).

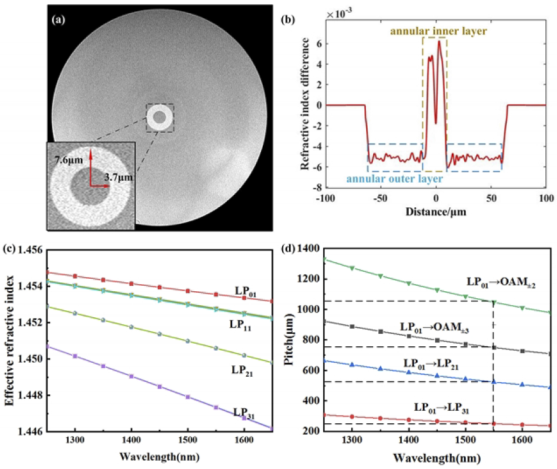

Fig. 1. (a) Fiber end face of RCF observed by SEM; (b) refractive index distribution of the RCF; (c) effective refractive index of the LP_{01}, LP_{11}, LP_{21}, and LP_{31} modes as a function of wavelength; (d) dispersion curve of resonant wavelength with respect to grating pitch for coupling the LP_{01} mode to LP_{21}, LP_{31}, ±2nd-order OAM mode, and ±3rd-order OAM mode from 1250 nm to 1650 nm.

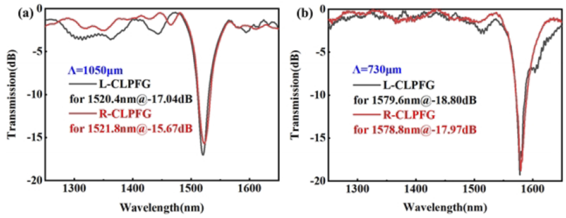

Fig. 2. Transmission spectra of the (a) CLPFG1s and (b) CLPFG2s.

According to the simulation results in Fig. 1(d), to realize the excitation of ±2nd-order and ±3rd-order OAM modes at 1550 nm, CLPFG1s with a pitch of 1050 µm and CLPFG2s with a pitch of 730 µm were fabricated by using a CO_2 laser to inscribe helical curves on the axis [17] of the RCF under a power of 447 mW. The light output from an amplified spontaneous emission light source (ASE) enters an optical spectral analyzer (OSA) after passing through single-mode fiber jumper1 (SMFJ), CLPFG, and SMFJ2 in turn. The energy of the high-order mode was lost in SMFJ2 and was not collected by OSA. Thus, the transmission spectra of CLPFGs were recorded with the OSA.

Figures 2(a) and 2(b) show the transmission spectra of CLPFG1s and CLPFG2s, respectively. The resonant wavelength and depth of the L-CLPFG1, R-CLPFG1, L-CLPFG2, and R-CLPFG2 were 1520.4 nm and 17.04 dB, 1521.8 nm and 15.67 dB, 1579.6 nm and 18.80 dB, and 1578.8 nm and 17.97 dB, respectively. For all CLPFGs, the grating length was 1 cm. The CLPFG conversion efficiency was as high as 98.7% and the insertion loss was as low as 0.5 dB.

The annular intensity distribution, spiral phase, and polarization characteristics of excited modes in CLPFG1s with pitch of 730 µm and CLPFG2s with pitch of 1050 µm were investigated by using a detection system based on the principle of spherical wave interference shown in Fig. 3(a). The incident light emitted from a tunable laser (TL) was divided into two beams by a 3-dB coupler. One beam was used as the reference light. The

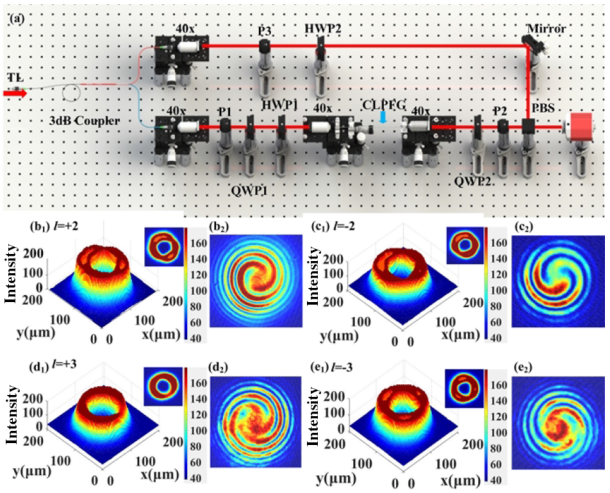

Fig. 3. (a) Setup for exploring characteristics of the mode excited in CLPFGs; (b_1), (c_1), (d_1), (e_1) the intensity distribution and (b_2), (c_2), (d_2), (e_2) interference diagram in CLPFGs.

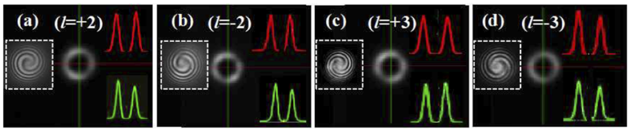

Fig. 4. Longitudinal and transverse intensity distribution detection results of (a) + 2nd-, (b) −2nd-, (c) +3rd-, and (d) −3rd-order OAM modes by CCD. The red and green waveforms represent the longitudinal and transverse intensity distribution, respectively. The interference diagram of each mode is in the white dashed frame.

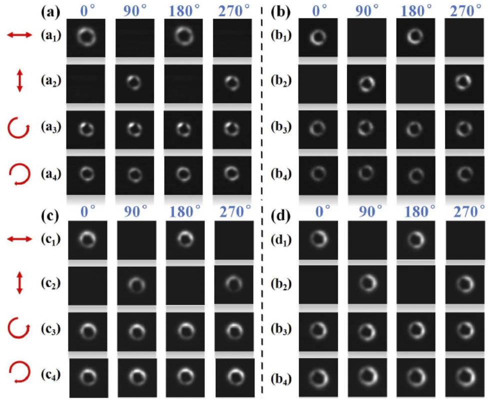

Fig. 5. Polarization characteristic of (a) + 2nd-order OAM mode excited in L-CLPFG1, (b) −2nd-order OAM mode excited in R-CLPFG1, (c) +3rd-order OAM mode excited in L-CLPFG2, and (d) −3rd-order OAM mode excited in R-CLPFG2 at the resonant wavelength. The icons in the leftmost column are the $LP^{\parallel}, LP^{\perp}$, LCP, and RCP state incident light from top to bottom, respectively.

other beam was injected into CLPFGs for generating the high-order mode. Then, the two beams were combined and interfered at the beam combiner. The annular intensity distribution and interference pattern of the two beams were recorded through a CCD. Polarizer (P1) and a quarter-wave plate (QWP1) were used to generate incident light with an arbitrary polarization state. P2 was used to analyze the polarization characteristics of excited modes in CLPFGs and P3 was used to filter unwanted stray light. Half-wave plates (HWP1 and HWP2) were used for changing the vibration direction of light. When the reference beam was blocked, the annular intensity pattern could be observed in Figs. 3(b_1), 3(c_1), 3(d_1), and 3(e_1). By identifying the color distribution, it can be observed that the ±2nd- and ±3rd-order OAM modes had uniform annular intensity distribution and each part was relatively equal. Figure 3 shows the spiral interference patterns in the CCD, where Figs. 3(b_2), 3(c_2), 3(d_2), and 3(e_2) correspond to L-CLPFG1, R-CLPFG2, L-CLPFG1, and R-CLPFG2, respectively. The excitation of +2nd-, −2nd-, +3rd-, and −3rd-order OAM modes in CLPFG was further demonstrated successfully. Furthermore, the +2nd- and +3rd-order OAM modes were excited in L-CLPFG while the −2nd- and −3rd-order OAM modes were excited in R-CLPFG, which indicated the chiral direction of the OAM mode was determined by the modulation direction of CLPFG. It is worth emphasizing that the light output from the CLPFGs at the non-resonant wavelength was still a fundamental mode. In addition, the roundness of the excited ±2nd- and ±3rd-order OAM modes could be calculated by the equation $O = 4 \times \pi \times A/P^2$, where A and P represented the area and perimeter of the closed profile, respectively. The roundness of the excited ±2nd- and ±3rd-order OAM modes were calculated. Result showed that the roundness of the outer and inner ring of +2nd-, −2nd-, +3rd-, and +3rd-order OAM modes were 0.87 and 0.91, 0.9 and 0.91, 0.87 and 0.93, and 0.87 and 0.9, respectively (the closer the roundness is to 1 means the rounder the closed contour).

To further investigate the intensity distribution of excited OAM modes, the longitudinal and transverse intensity distribution can be detected directly by a CCD, as shown in Figs. 4(a), 4(b), 4(c), and 4(d). From the results of the longitudinal and transverse intensity waveform, the intensity distribution was relatively uniform in the transverse and longitudinal directions. Note that the components of other OAM modes had a negative effect on the uniform annular intensity distribution. Moreover, Fig. 5 shows the polarization characteristics of excited ±2nd- and ±3rd-order OAM modes in CLPFGs at resonant wavelength. Here, $LP^{\parallel}$ and $LP^{\perp}$ represent the vibration direction parallel and perpendicular to the transparent axis of P2. By adjusting the transparent axis of P2 and fast axis of QWP2, left circularly polarized (LCP) state and right circularly polarized (RCP) state incident light were produced. The intensity distributions of excited +2nd-, −2nd-, +3rd-, and −3rd-order OAM mode in CLPFGs are shown for $LP^{\parallel}$ state incident light in Figs. 5(a_1), 5(b_1), 5(c_1), and 5(d_1), respectively. As the P2 transparent axis was rotated at 90° intervals, the intensity periodically alternated between bright and dark fringes. The $LP^{\parallel}$ state incident light was transformed into $LP^{\perp}$ light by adjusting the HWP2. A similar result was observed for the *textrmLP*$^{\perp}$ state incident light, but with a phase delay of $\pi/2$, which is shown in Figs. 5(a_2), 5(b_2), 5(c_2), and 5(d_2). This showed that the excited OAM modes maintained the same linearly polarized state as that of incident light.

For LCP and RCP state incident light, the evolution of these intensity profiles was observed with the rotation of P2. The annular intensity distribution of +2nd-, −2nd-, +3rd-, and −3rd-order OAM modes remained constant in Figs. 5(a_3), 5(a_4), 5(b_3), 5(b_4), 5(c_3), 5(c_4), 5(d_3), and 5(d_4), which indicated the excited OAM modes were circularly polarized. The combination of QWP2 and P2 were used to detect the circular polarized rotation detection of OAM modes. The light emitted from CLPFG passed through

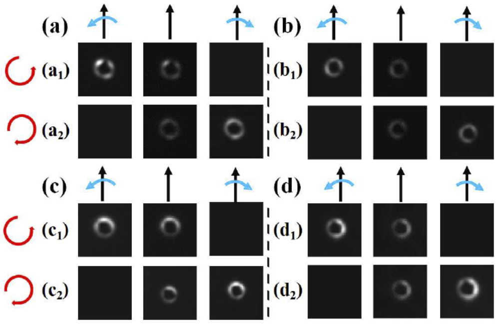

Fig. 6. Circular polarized rotation detection of (a) L-CLPFG1, (b) R-CLPFG1, (c) L-CLPFG2, and (d) R-CLPRG2, for LCP and RCP state incident light. The black and blue arrow represent the fast axis direction of QWP2 and the transparent axis of P2, respectively.

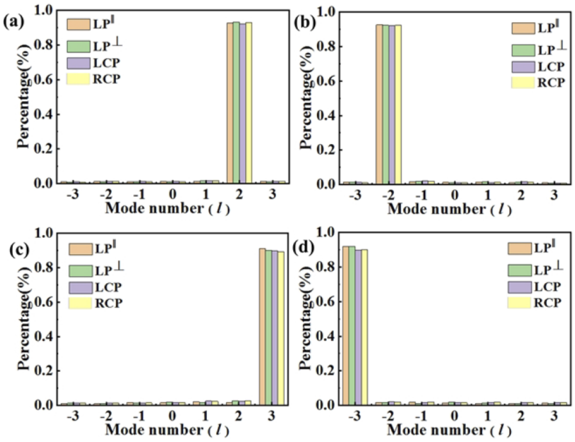

Fig. 7. Purity of the excited (a) +2$^{\text{nd}}$-, (b) −2$^{\text{nd}}$-, (c) +3$^{\text{rd}}$-, and (d) −3$^{\text{rd}}$-order OAM mode in the CLPFGs for LP$^\parallel$, LP$^\perp$, LCP, and RCP state incident light.

the combination where the fast axis of QWP2 was parallel to the light transmission axis of P2. As shown in Figs. 6(a$_1$), 6(b$_1$), 6(c$_1$), and 6(d$_1$), both in L-CLPFG and R-CLFPG, the intensity of the output light became bright with clockwise rotation of P2 for LCP state incident light. With anticlockwise rotation of P2, the output light became dark. For RCP state incident light in Figs. 6(a$_2$), 6(b$_2$), 6(c$_2$), and 6(d$_2$), the intensity of output light became bright and dark, with anticlockwise and clockwise rotation of P2, respectively. This indicated that the circular polarized rotation of the excited OAM mode was consistent with the incident light.

The purity of excited OAM modes in L-CLPFG1, R-CLPFG1, L-CLPFG2, and R-CLPFG2 were investigated by the mode decomposition method, as recorded in Fig. 7. For LP$^\parallel$, LP$^\perp$, LCP, and RCP state incident light, the results showed that the primary component was the +2$^{\text{nd}}$-order OAM mode in L-CLPFG1, and the mode purity was 92.5%, 93.2%, 91.9%, and 92.8%, respectively. The primary component in R-CLPFG1 was the −2$^{\text{nd}}$-order OAM mode with a purity of 92.4%, 92.1%, 92.0%, and 92.2%, respectively. Simultaneously, the purity of +3$^{\text{rd}}$-and −3$^{\text{rd}}$-order OAM modes in L-CLPFG2 and R-CLPFG2 were 91.1%, 90.0%, 89.7%, 89.9% and 91.7%, 91.8%, 89.8%, 89.9%, respectively. The results also proved the topological charge number of excited OAM modes in each CLPFG in Fig. 5, for LP$^\parallel$, LP$^\perp$, LCP, and RCP state incident light.

We have designed and fabricated CLPFGs in an RCF. The CLPFGs have low insertion loss, high mode conversation efficiency, and short grating length. In CLPFGs, the ±2$^{\text{nd}}$- and ±3$^{\text{rd}}$-order OAM modes were directly excited with a uniform annular intensity distribution, relatively high mode purity, and polarization independence. The high purity and uniform annular intensity distribution of the OAM mode may reduce the intermode cross talk effectively. Excitation of the helical phase in CLPFG is independent of the polarization state of incident light, which is conducive to the simultaneous multiplexing of the OAM mode and polarization. Therefore, the proposed OAM generator can be directly applied to HCOFCS, which is beneficial for the development of space division multiplexing technology.

Funding. Foundation of Shenzhen University (201904); Science Foundation of Guangdong Province (2022A1515010183); National Natural Science Foundation of China (61875134, 62005169).

Disclosures. The authors declare no conflicts of interest.

Data availability. Data underlying the results presented in this paper are not publicly available at this time but may be obtained from the authors upon reasonable request

REFERENCES

1. D. J. Richardson, J. M. Fini, and L. E. Nelson, Nat. Photonics **7**, 354 (2013).
2. J. Wang, S. Chen, and J. Liu, APL Photonics **6**, 060804 (2021).
3. S. Ramachandran and P. Kristensen, Nanophotonics **2**, 455 (2013).
4. Z. Zhang, J. Gan, X. Heng, Y. Wu, Q. Li, Q. Qian, D. Chen, and Z. Yang, Opt. Express **23**, 29331 (2015).
5. R. M. Nejad, K. Allahverdyan, P. Vaity, S. Amiralizadeh, C. Brunet, Y. Messaddeq, S. LaRochelle, and L. A. Rusch, J. Lightwave Technol. **34**, 4252 (2016).
6. N. R. Heckenberg, R. Mcduff, C. P. Smith, and A. G. White, Opt. Lett. **17**, 221 (1992).
7. X. He, J. Tu, X. Wu, S. Gao, L. Shen, C. Hao, Y. Feng, W. Liu, and Z. Li, Opt. Lett. **45**, 3621 (2020).
8. Y. Zhao, Z. Liu, Y. Liu, C. Mou, T. Wang, and Y. Yang, Opt. Lett. **44**, 5905 (2019).
9. K. Ren, L. Ren, J. Liang, L. Yang, J. Xu, D. Han, Y. Wang, J. Liu, J. Dong, H. He, and W. Zhang, Opt. Express **29**, 8441 (2021).
10. J. Yu, C. Fu, Z. Bai, and Y. Wang, J. Lightwave Technol. **39**, 1416 (2021).
11. N. Bozinovic, S. Golowich, P. Kristensen, and S. Ramachandran, Opt. Lett. **37**, 2451 (2012).
12. K. Yang, Y.-G. Liu, Z. Wang, Y. Li, Y. Han, H.-W. Zhang, and B.-W. Mao, Opt. Fiber Technol. **55**, 102155 (2020).
13. H. Zhao and H. Li, Photonics **8**, 106 (2021).
14. H. Zhao and H. Li, Opt. Lett. **44**, 5370 (2019).
15. M. Napiorkowski and W. Urbanczyk, Opt. Lett. **43**, 395 (2018).
16. G. Shvets, S. Trendafilov, V. I. Kopp, D. Neugroschl, and A. Z. Genack, J. Opt. A: Pure Appl. Opt. **11**, 074007 (2009).
17. Z. Bai, Y. Wang, Y. Zhang, C. Fu, S. Liu, M. Li, C. Liao, Y. Wang, J. He, and Y. Wang, IEEE Photonics Technol. Lett. **32**, 418 (2020).